Effect of UV irradiation time on the structure and optical properties of Rose Bengal thin films

Zeyada HM[a,*], Youssif MI[a], El-Ghamaz NA[a], Aboderbala MEO[a,b]

[a] Department of physics, Faculty of science,34517, University of Damietta. Egypt
[b] Department of physics, Faculty of science, AlJabl Al Gharbi University, Libya

* Corresponding author: (Fax: +20572403868, Tel.:+20572404097, E-mail address: hzeyada@gmail.com)

Abstract

Optical properties of pristine and UV irradiated Rose Bengal (RB) films have been investigated using transmittance and reflectance methods. The refractive index (n) and extinction coefficient (k) of RB films were directly calculated from absolute values of transmission and reflection spectra. Single oscillator parameters and the Drude model of free carrier absorption have been used for the analysis of refractive index dispersion. The fundamental absorption edge data were analyzed within the frame work of the band- to-band electron transitions theory. The thickness of RB films has no influence on absorption and refractive indices in the investigated thickness range and within the experimental error. UV irradiation caused a structural transformation of amorphous pristine film to polycrystalline RB film, which resulted in the decrease of absorption coefficient, energy gap and refractive index. The optical functions and their dependence on UV exposure time were directly calculated from the spectral distribution of dielectric constant.

Keywords: Rose Bengal; Thin films; UV irradiation; Optical properties; Optical functions

Introduction

Rose Bengal (2,4,5,7- tetraiodo- 3, '4',5',6'-tetrachlofluorescein) is a tetraiodo-substituted dye of the xanthene's class of dyes. It has peculiar photophysical and photochemical properties, such as: high absorption in all solvents in which it is soluble, high intersystem crossing yield and it shows some fluorescence, it is a photodynamic sensitizer, it bleaches slowly in protic, polar solvents and its spectrum is most diagnostic of its immediate environment. Due to the richness in its properties, it has assumed a peculiar role in different fields of disciplines such as applications in bulk heterojunction solar cells (Sharma *et al*., 2009) and dye- sensitized solar cells (Pradhan *et al.*, 2007; Roy *et al*., 2008).It is used as a photo sensitizer for the enhancement of conversion efficiency and storage capacity of photo galvanic cells (Gangotri and Bhimwal, 2010), It sensitized TiO_2 film electrode (Zhao *et al*., 1997). Rose Bengal water solutions quenched by potassium iodide can be used to measure instrument response functions of single photon detectors in the orange-red wavelength region (Szabeiski *et al*., 2009). RB is used as a photo sensitizer in dye

sensitized photo chemical cells (Jana., 2000; Bahadur and Roy, 1999). And it also has medical and biological applications (Kim *et al*., 2011; Wang *et al*., 2013; Chang *et al*., 2013).

Despite the numerous applications of Rose Bengal dye in various areas, information on the optical and dielectrical properties in bulk and thin film forms is not yet reported. In semiconductor device fabrication materials are usually provided as thin films. In this work, we report for the first time, on the influence of film thickness and ultraviolet exposure time on structure formation, optical and dielectrical properties and optical functions of RB films prepared by the spin coating technique.

Experimental procedure

Rose Bengal, RB, $(C_{20}H_2Cl_4I_4Na_2O_5)$ was obtained from Aldrich and used as-supplied. The Chemical structure of RB is shown in Fig. 1. RB is dissolved in absolute ethyl alcohol (99.9%) up to saturation. Homogenous thin films of Rose Bengal (RB) are prepared by the conventional spin coating technique onto pre-cleaned optical flat quartz substrates at room temperature for optical measurements and onto pre-cleaned KBr substrates for the Fourier transform infrared (FTIR) measurements. Cleaned ordinary glass slides were used as substrates for depositing films for X-ray diffraction (XRD) analysis. The substrates are fixed to the stage of the spin coater and the rotating speed is adjusted to about 2800 rpm. The film thickness was determined optically by the Lloyd's method (Hamza *et al*., 2003).The thickness of the produced thin films is measured and found to be in the range 110-500nm. The samples were irradiated with a UV lamp (Cole-Parmer model 9815-series Lamps 100 watts). The instrument operates with a UV output at 254nm. FTIR, spectra were recorded using Perkin-Elmer 1340 spectrophotometer. Structural analysis of the powder and thin films is performed at room temperature using X-ray diffraction system (Philips X' pert) with filtered CuK$_\alpha$-radiation (λ =1.5405 Å). The diffraction system was used to investigate the formed phase in the angle range 4–60°.The applied voltage and tube current were 40 kV and 30 mA, respectively. A double beam spectrophotometer (JASCO model V-570-UV/Vis./NIR, Japan) was used for measuring the transmittance, $T (\lambda)$, and reflectance, $R(\lambda)$, of thin films in the wavelength range 200-2500nm. The measurements were carried out at room

temperature and the light beam was adjusted nearly at normal incidence. The absolute values of $T (\lambda)$ and $R(\lambda)$ were used to calculate the optical constants according to the relations (El-Nahaas *et al*., 2002).

$$T(\lambda) = \left(\frac{I_{ft}}{I_q}\right)(1 - R_q),$$ (1)

$$R(\lambda) = \left(\frac{I_{fr}}{I_{Al}}\right)R_{Al}\left[1 + (1 - R_q)^2\right] - T^2 R_q,$$ (2)

Where I_{ft} and I_q are the intensities of light passing through film quartz system and reference quartz substrate, respectively. The intensities of the light reflected from the sample and from the reference mirror are I_{fr} and I_{Al}, respectively. The reflectance of Al mirror is R_{Al} and R_q is the reflectance of the quartz substrate.

The refractive index, n, absorption index, k, and absorption coefficient, α, can be calculated using the absolute values $R(\lambda)$ and $T(\lambda)$ according to the following relations (Zeyada *et al*., 2012).
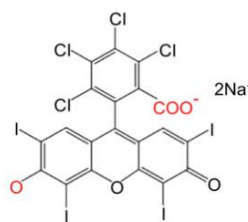

Fig 1. The molecular structure of Rose Bengal.

$$\alpha = \left(\frac{1}{d}\right)\ln\left[\frac{(1-R)^2}{2T} + \sqrt{\frac{(1-R)^4}{4T^2} + R^2}\right]$$ (3)

$$k = \frac{\alpha\lambda}{4\pi}$$ (4)

$$n = \frac{(1+R)}{(1-R)} + \sqrt{\left(\left(\frac{4R}{(1-R)^2}\right) - k^2\right)}$$ (5)

Where d is the thickness of the film and λ is the wavelength of the incident light on the sample. The refractive index, n, can be calculated from the relation (El-Nahass and Youssef, 2010).

Since the thickness of the film (d) is previously determined, then the computation can be carried out and the values of n, k and α can be obtained. The experimental errors are taken into account as follows: ±1% for T and R calculations, ±3% for refractive index, ±2.5% for

absorption index and±2.5% for film thickness measurements (Konstantinov *et al*., 1998).

Results and Discussion

A comparison between the FTIR spectrum of the as received RB powder, RB in the as prepared thin film form and UV irradiated thin film condition is shown in Fig. 2. The absorption peaks are assigned and listed in Table 1. In all conditions, there are small shifts in the peak position of the absorption peaks and this does not prevent us from concluding that there is no change in the chemical bonds of RB resulting either from spin coating or irradiation process.

Table 1. Assignment of transmission peaks for RB in powder, pristine and UV irradiated (180 min.) thin films

Powder $\bar{v}$ (cm^{-1})	Pristine film $\bar{v}$ (cm^{-1})	Irradiated film (180 min.) $\bar{v}$ (cm^{-1})	Assignment
456.29	451.422	452.78	C — I
516.33	511.46	513.64	C —Cl
567.44	567.44	566.84	C — Cl
614.51	614.51	617.06	C — Cl
657.51	657.51	658.57	C — Cl
760.55	760.55	761.35	C — Cl
952.855	952.85	953.51	C— C stretching vibration
1120.81	1115.94	1118.89	C — H in plane bending vibration
1171.2	1171.92	1169.9	C — H in plane bending vibration
1244	1240.08	1240.42	C — H in plane bending vibration
1335.015	1339.07	1338.51	C=C stretching vibration
1455.1	1450.23	1451.67	C=C stretching vibration
1493.23	1489.17	1493.18	C=C stretching vibration
1549.22	1553.27	1553.78	C=C stretching vibration
1613.37	1617.31	1612.36	C=O stretching vibration

The weak peak at 451-456 cm^{-1} is assigned as C-I and the vibration modes in the range 567-760 cm^{-1} are due to multi C-Cl bonds. The absorption peak at 1613-1617 cm^{-1} is due to C=O stretching vibration.The average crystallite size, *D*, can be

calculated using the well-known Scherer's equation (Cullity, 1978).

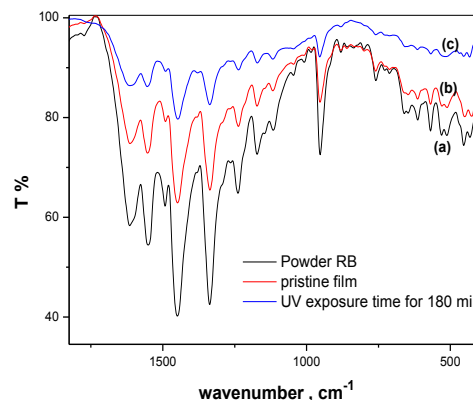$$D = \frac{0.95\lambda}{\gamma \cos\theta}, \qquad\qquad (6)$$

Fig 2. FTIR spectra of RB, (a) powder form, (b) pristine film and (c) UV-irradiated film for 180 min.
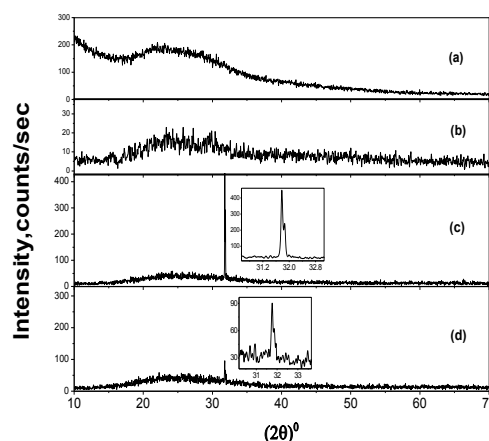

Fig 3. XRD patterns of RB, (a) Powder form, (b) Pristine thin film, (c) UV-irradiated film for 90 min and (d) UV-irradiated film for 180 min.

Where γ the width at the half- maximum peak intensity, measured in radians, λ is the X-ray wavelength and θ is the Bragg's angle. The x-ray diffraction (XRD) patterns of RB in the powder from, pristine and UV-irradiated thin films (exposure times are 90 and 180 min) are shown in Fig. 3. As can be observed from Fig. 3 (a,b), there is a halo around 2θ≈23°indicating that both of the powder and the pristine thin films of RB have amorphous structure. Fig. 3c shows that the amorphous structure of the pristine thin film crystallizes into a single polycrystalline phase upon UV exposure for 90 minutes. Fig. 2 and Table 1 illustrate that the amorphous phase of RB

film has the same chemical bonds as that of polycrystalline phase and this indicates that polymorphous polycrystallization occurred, where atoms in the disordered state jump to crystal front and those in clusters change their orientation to match the growing crystal and deposit onto the crystal front. The determined crystallite size of RB film exposed to UV irradiation time of 90 minutes is 230 nm. Increasing UV irradiation time to 180 minutes recrystallizes the polycrystalline phase of RB film (Fig. 3(c)) into smaller grains of about 144 nm in size as shown in Fig. 3 (d).

Optical properties

Determination of optical constants of the as prepared RB thin films

The influence of film thickness on spectral behavior of $T(\lambda)$ and $R(\lambda)$ for the pristine RB films is depicted in Fig. 4. The determined film thicknesses are 110, 250 and 500 nm. Inspection of Fig. 4 clearly shows that there is no influence of film thickness on spectral behavior of $T(\lambda)$ and $R(\lambda)$ within the investigated thickness range and within the experimental error. The sum of $T(\lambda)$ and $R(\lambda)$ is approximately equal to unity at $\lambda \geq 600$ nm indicating a non-absorbing region while at wavelengths $\lambda \leq 600$ nm, the sum of $T(\lambda)$ and $R(\lambda)$ is much less than unity indicating that the RB is a good absorber of light in this region of the spectrum. We conclude also that light is not dispersed and this indicates that the films are homogenous and optically flat. A transmission band is observed in the wavelength range 272- 496nm indicating that RB films can be used as optical filters.

The optical properties of different materials can be fully characterized by the complex refractive index, n^*, where $n^* = n - ik$. In general, the real part, n, is related to the dispersion, while the imaginary part (absorption index), k, provides a measure of dissipation rate of the electromagnetic wave in the dielectric medium. The calculation of n and k was carried out for films with different thicknesses ranging from 110 to 500 nm. The values of the refractive and absorption indices for RB thin films are computed using the absolute values of transmittance and reflectance. The results depicted in Fig. 5 represent the average values of n and k for the above mentioned thicknesses at given wavelength. The calculations indicated that the optical constants (n, k) do not depend on film

thickness of RB films. This result has been observed for some organic semiconductor materials (El-Menyawy *et al.*, 2013; Zeyada *et al.*, 2012; El-Nahass *et al.*, 2004).
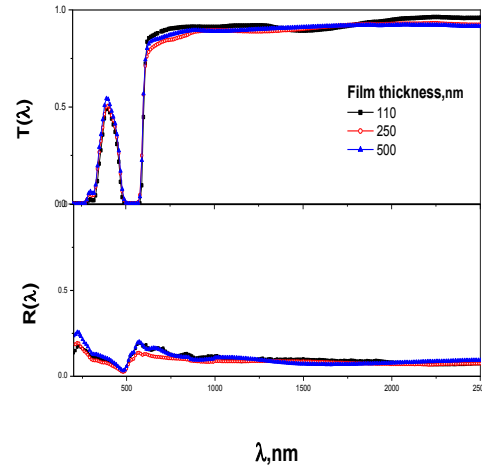

Fig 4. Spectral distribution of transmittance, T( ), and reflectance, R( ) for the pristine RB thin films
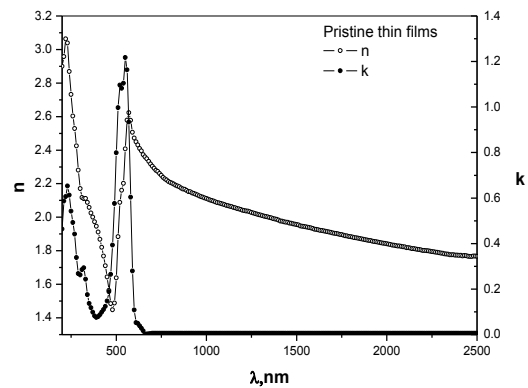

Fig 5. Spectral distribution of refractive index, n, and extinction coefficient, k, for pristine RB thin films.

The spectral behavior of n shows a normal dispersion at $\lambda > 600$ nm and an anomalous dispersion at $\lambda < 600$ nm. The dispersion curve (Fig. 5) shows two dispersion peaks and two shoulders in the ultraviolet and visible region of spectra. These features can be explained using the multioscillator model. The spectral behavior of n in the normal dispersion region can be explained by adopting the single oscillator model. In this region, we can deduce optical functions and oscillator parameters at high frequencies from data of refractive index. The results of k show two absorption peaks in the UV region and a doublet peak in the wavelength range 479 - 650 nm. The doublet peak in the visible region of

26

spectra has been reported for RB by many authors (Sharma *et al*., 2009; Roy *et al*., 2008; Pradhan and Pal 2004). All peaks in extinction absorption curve are attributed to the electronic transitions from bonding to anti-bonding molecular orbital (multi oscillator model) (El-Korashy *et al*., 2003; El-Mallah *et al*., 2010).

Effects of UV irradiation time on the optical constants of RB thin films

The effect of UV irradiation time, 90 and 180 min., on the spectral behavior of *T(λ)* and *R(λ)* for the RB thin film of thickness 110 nm is presented in Fig. 6. Generally, the irradiation process reduces the values of *T* and *R* over all the spectrum. No new peaks were observed in the T and *R* in the absorption region of spectrum. Therefore, UV irradiation has no effect on the transmittance and reflectance properties of the films in the absorption region of the spectrum.

Absorption characteristics of films

The spectral dependence of absorption coefficient, α, for UV irradiated RB thin films, in comparison with that of pristine thin films, is illustrated in Fig. 7. It is clear that the pristine RB films have high absorption coefficient (6×10^5 cm^{-1} at 2.24eV) in the UV-visible region of the spectrum. This indicates that the type of electron transition in the RB films is a direct one. UV irradiation process reduces the value of α all over the spectrum. The decrease of α upon UV irradiation can be attributed to the change in the microstructure of RB film from amorphous, for as-prepared films, to polycrystalline structure for irradiated films as shown in Fig. 3. The observed increase in crystallite size for UV irradiated film for 90 minutes decreases its absorbance, this result is in good agreement with previous work of Hindeleh, et al. (1990).

The transmittance and absorbance of a liquid depends on the molar concentration, C_M, light path length in centimeters, L, and molar absorptivity, ξ_{molar} for the dissolved solution (Dean, 1992).

$$A_\lambda = \xi_{molar}\, C_M\, L \qquad (7)$$

Beer's law states that molar absorptivity is constant and the absorbance is proportional to the concentration of the dissolved substance at the specified wavelength (λ) (Weast, 1975). The molar absorptivity is commonly called molar extinction coefficient and it has units of mol^{-1} cm^{-1}. The molar extinction coefficient, ξ_{molar}, is a measure of the ability of a molecule to absorb light in non-solid molecular media, can be obtained in terms of the absorption coefficient. If a solid has a concentration of N molecules per unit volume then ξ_{molar} can be written as (Schechtman and Spicer, 1970).
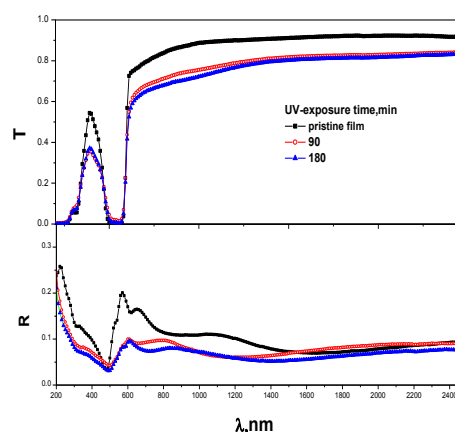

Fig 6. Spectral distribution of transmittance, T( ) and reflectance, R( ) for UV irradiated RB thin films with different exposure times.

$$\xi_{molar} = \frac{10^{-3}}{Ln10}\frac{N_a}{N} = \frac{10^{-3}}{Ln10}\frac{M_w}{\rho}\alpha = G\alpha \qquad (8)$$

Where N_a is Avogadro's number, M_w is RB molecular weight, ρ is the material density and G is a constant. The molar extinction coefficient spectra for the as-prepared and UV-irradiated RB thin films, with a thickness of 110 nm are depicted in Fig. 8. The as-prepared film exhibited high molar extinction coefficient and the major peak is split into two peaks (B_x and B_y).The splitting of the band depends on the distance between the molecules, the angle of the transition dipole moments between neighboring molecules and number of interacting molecules (Schomaker *et al*., 1959). Fig. 8 shows that the value of ξ_{molar} decreases with increasing UV exposure time. The peaks B_x and B_y exchange their peak intensity when UV exposure times exceeds 20 minutes. The remarkable high molar extinction coefficient of 5.4×10^4 (mol.cm)$^{-1}$ at wave number 1.9×10^4 cm^{-1} for RB films is comparative with those of other organic dyes (Zeyada *et al*., 2012; Jiang *et al*., 2008). High

molar extinction coefficient and broad absorption band are required in materials to increase the photocurrent density and improve the solar conversion efficiency.
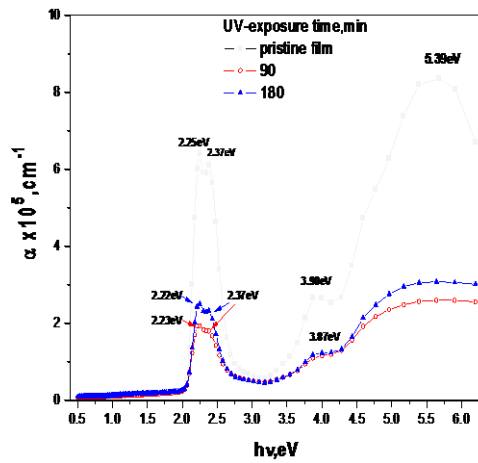

Fig 7. Spectral distribution of absorption coefficient, of RB thin films with different exposure times to UV irradiation.

The molar extinction coefficient spectrum usually allows calculating two spectral parameters, namely the oscillator strength, f, and the electric dipole strength, q^2, using the following expressions (Kumar et al., 2000).

$$f = 4.32 \times 10^{-9} \int \xi_{molar}(\nu) d\nu \qquad (9)$$

and

$$q^2 = \frac{1}{2500} \xi_{molar}(\frac{\Delta\lambda}{\lambda_{max}}) \qquad (10)$$

Where $\Delta\lambda$ is the band width at half maximum of the absorption peak and λ_{max} is the wavelength at maximum absorption.
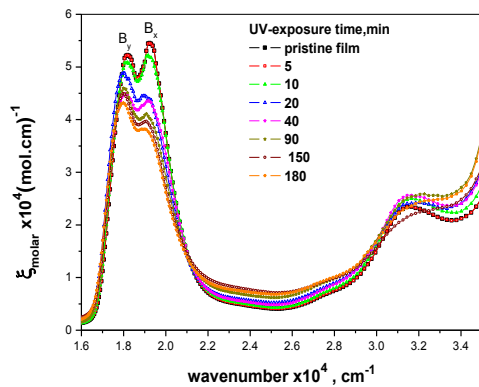

Fig 8. Spectral distribution of molar extinction coefficient for RB thin films with different exposure times to UV irradiation.

The calculated results of oscillator strength, *f,* and electric dipole moment, q^2, for the as-prepared and UV-irradiated RB thin films are listed in Table 2. The two absorption peaks, B_x and B_y, are due to splitting in the band and have high intensity, this results in large values of oscillator strengths which are due to parallel electric dipoles (Baerends *et al.*, 2002). Therefore, the increase in spectral parameters is related to the increase of both intensity and broadening of the absorption band. The UV irradiation decreases the intensity of the absorption bands, as shown in Fig. 8, since it rearranges few of electric dipoles from parallel into opposite direction and consequently the oscillator and electric dipole strengths are decreased.

The study of absorption coefficient of a material, at and near the absorption edge, provides valuable information about its band structure. The dependence of absorption coefficient of a material, on the incident photon energy has been formulated by Tauc's relation (Tauc, 1974). As:

$$\alpha h\nu = B(h\nu - E_g^{onset})^x, \qquad (11)$$

Where *B* is a constant related to the electronic transition probability and *x* is the power which characterizes the type of transition process, namely *x*=1/2 and 3/2 for direct allowed and forbidden transitions, respectively, and *x*=2 and 3 for indirect allowed and forbidden transitions, respectively. The best fit for the data is found for x=2, indicating that the dominant transition is indirect allowed one. Fig. 9 presents the spectral distribution of $(\alpha h\nu)^{1/2}$ as a function of incident photon energy. The value of the energy gap is obtained by extrapolating the straight portion of the curve to intercept the abscissa axis.

Table 2. Parameters of molar extinction coefficient for pristine and UV irradiated RB thin films

UV-irradiation time, min	f	$q^2(\text{Å})^2$
Pristine film	0.82	1.448
5	0.88	1.443
10	0.81	1.374
20	0.73	1.193
40	0.76	1.102
90	0.57	1.093
150	0.49	1.062
180	0.64	1.006

The onset energy gap corresponds to the optical absorption, formation of vacancies, interstials, Frenkel pairs and dislocations in the

films (Tsiper *et al*., 2002). The energy gap is the energy gap between HOMO-LUMO bands (Zhokhavets *et al*., 2003). The values of $E_g^{.onset}$ and $E_g^{.}$ for pristine and UV irradiated RB thin films are tabulated in Table 3. These changes in energy gaps can be attributed to the crystallization process which occurred in RB films upon UV-irradiation as shown previously in Fig. 3. As can be observed from Table 3 and Fig. 9, the UV- irradiation process decreases $E_g^{.onset}$ and $E_g^{.}$. Increasing exposure time of UV irradiation has no influence on energy gap.

Table 3. Dependence of optical and fundamental energy gap of RB films on UV exposure time

Exposure time , min.	E_g^{onset} , eV	$E_g^{.}$, eV
Pristine film	2.02	2.59
90	1.98	2.33
180	1.98	2.33

Table 4. Dispersion parameters of pristine and UV irradiated RB thin films

UV irradiation time	ε_L	ε_∞	$(N/m^*)\times 10^{55}$, $m^{-3}kg^{-1}$	E_o (eV)	E_d (eV)
Pristine film	3.613	3.272	3.325	3.091	7.024
90 min	3.222	2.951	2.746	3.106	6.061
180 min	3.049	2.777	3.172	3.395	6.034

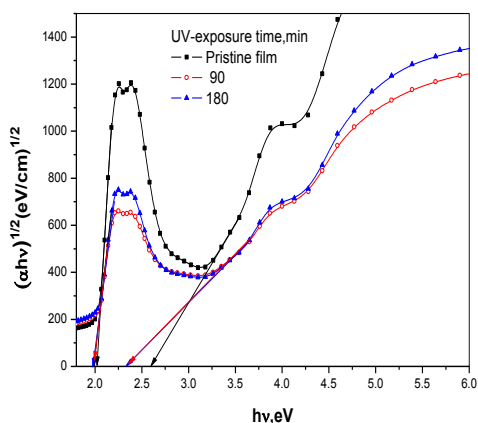**Fig 9.** Relation between (h)1/2 and h for RB thin films with different exposure times to UV irradiation.

Dispersion characteristics of RB films

The spectral distribution of the refractive index, n, for pristine and UV irradiated RB films is illustrated in Fig. 10. It shows an anomalous

dispersion in the wavelength range < 600 nm and exhibits three dispersion peaks and a shoulder for RB films; these are attributed to electronic transition across π–π* orbital (Davydov, 1971). The normal dispersion is observed for wavelength > 600nm and in this wavelength range we can deduce the values of optical functions from the data of refractive index.UV irradiation reduces the value of the refractive index all over the spectra. The decrease of the refractive index with UV irradiation is related to the decrease of mass density of RB films (Andreas *et al*., 2005). Such behaviour has been reported in other organic semiconductor thin films (El-Nahass *et al*., 2011; El-Nahass *et al*., 2012; El-Nahass *et al*., 2011).
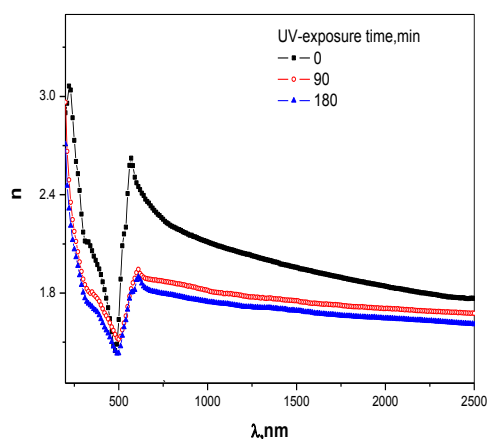

Fig 10. Spectral distribution of refractive index, n, for RB thin films with different exposure times to UV irradiation.

Wemple and Di-Domenico (1971) proposed the single oscillator model to explain the spectral dependence of refractive index in the transparent region of spectra, in this model the refractive index is related to the dispersion parameters by:

$$\frac{1}{n^2-1} = \frac{E_o}{E_d} - \frac{1}{E_oE_d}(h\nu)^2 \tag{12}$$

Where $h\nu$ is the photon energy, E_o the oscillator energy that gives quantitative information of the overall band structure of the material and E_d is the dispersion energy which is a measure of the strength of inter-band optical transition inside the material (Solomon *et al*., 1988). A plot of $(n^2-1)^{-1}$ versus $(h\nu)^2$ for RB films in the pristine and UV irradiated conditions is illustrated in Fig. 11. The oscillator energy, E_o, and the dispersion energy, E_d, are directly

determined from the slope $(E_oE_d)^{-1}$ of the linear portion of the curve and its intercept with ordinate axis (E_o/E_d). The values of E_o, E_d and ε_∞ are listed in Table 4. and they are influenced by UV-irradiation.

Dielectric characteristics

Dielectric function relates the electron transitions between bands of a solid to its structure, therefore we can obtain valuable information about the band structure of a solid from its dielectric spectrum. The real, ε_1, and the imaginary, ε_2, parts of the complex dielectric constant, ε^*, are given by(Edward, 1985):
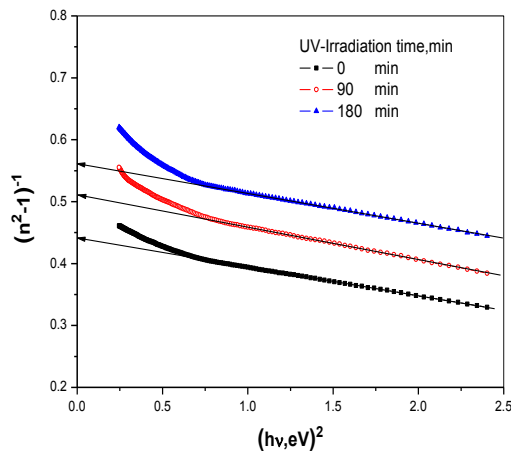

Fig 11. Relation between (n2-1)-1 and (h)2for RB thin films with different exposure times to UV irradiation.

$$\varepsilon_1 = n^2 - k^2 = \varepsilon_L - \left(\frac{e^2(N/m^*)}{4\pi^2 c^2 \varepsilon_o} \right) \lambda^2, \qquad (13)$$

$$\varepsilon_2 = 2nk \qquad (14)$$

where ε_L is the lattice dielectric constant, N/m^* is the ratio of carrier concentration to the effective mass, e is the electron charge, c is the speed of light in vacuum, and ε_o is the permittivity of free space. A graphical representation of n^2 as a function of λ^2 for the pristine and UV irradiated RB films is shown in Fig. 12. By extrapolating the linear part towards the shorter wavelength, the intercept with the ordinate axis (at $\lambda^2 = 0$) gives the value of ε_L and from the slopes of these lines the ratio N/m^* can be calculated. The calculated values of ε_L, ε_∞ ,N/m^* and the dispersion and oscillator energies

are given in Table 4. UV irradiation influences the values of dispersion parameters in comparison to those values of pristine RB film. The value of ε_L differs from the value of ε_∞ and this may be attributed to the structural changes occurred on RB films resulting from UV irradiation. N/m* varies with UV exposure times and therefore ε_L and ε_∞ depend on the UV exposure time.
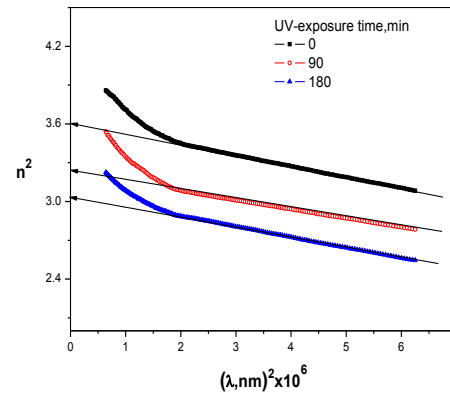

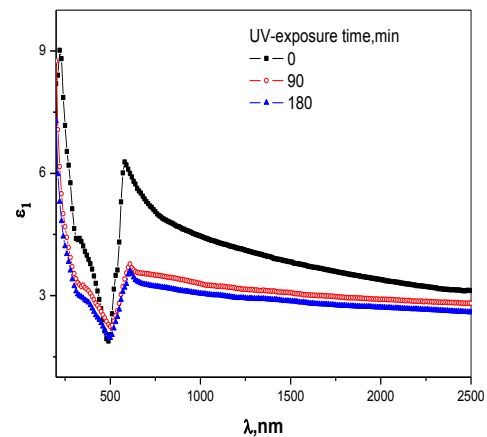**Fig 12.** Relation between n2 and   for RB thin films with different exposure times to UV irradiation.

Fig 13. Spectral distribution of for RB thin films with different exposure times to UV irradiation.

The spectral distribution of ε_1 and ε_2 is shown in Figs. 13 and 14, the values of ε_1 are larger than those of ε_2 at the same wavelength. The spectral distribution of ε_1 and ε_2 indicates the presence of different interactions between the incident photons and electrons in the RB film. These interactions affect the shapes of the curves and cause formation of peaks in the dielectric spectra. The decrease in ε_1 and ε_2 with increasing UV exposure time is related to

structural changes in RB films as shown in Fig. 3.

The real σ_1 and the imaginary σ_2 parts of the optical conductivity can be used to detect any further allowed interband optical transitions. The following relation expresses the complex optical conductivity σ^* in terms of σ_1 and σ_2 (Yakuphanoglu *et al*., 2004). As:

$$\sigma^* = \sigma_1 - i\,\sigma_2 \ , \tag{15}$$

where

$$\sigma_1 = \frac{\omega}{4}\varepsilon_2 \quad \text{and} \quad \sigma_2 = \frac{\omega}{4}\left(1-\varepsilon_1\right) \tag{15 a}$$

Fig. 15 illustrates the spectral distribution of σ_1 for RB thin films with different exposure times to UV irradiation. Increasing UV exposure time increases the value of σ_1 and this is attributed to variation of crystallite size with UV exposure time as shown in Fig.3. The onset energy gap is observed at 2.07 eV for pristine and UV irradiated film. The energy gap is observed at 2.85 eV for pristine film and at 2.48 eV for UV exposed film. These results are in agreement with those obtained from Fig.9 and confirm that the type of electron transition is an indirect allowed transition. For photon energy less than 2eV, σ_1 has a negligible value. UV irradiation has no influence on energy levels of RB but it influenced the onset and energy gaps.

microstructure changes in RB films upon UV exposure where it transformed from amorphous structure to polycrystalline as shown in Fig. 3.

Electron- energy-loss spectroscopy has been realized as an important probe for the dielectric response of solids and the intrinsic statistical nature of the particle penetrating phenomenon. The energy loss functions provide a complete description of the response of the material to ionizing particles or photons traveling either through its bulk or on its surface. The surface energy loss, SEL and the volume energy loss, VEL, are related to the related and imaginary parts of the dielectric constant by the following relationships (El- Nahass *et al*., 2003):

$$SEL = \frac{\varepsilon_2}{(\varepsilon_1+1)^2 + \varepsilon_2^2}, \tag{16}$$

$$VEL = \frac{\varepsilon_2}{(\varepsilon_1^2 + \varepsilon_2^2)} \tag{17}$$

Fig 15. Spectral distribution of σ1for RB thin films with different exposure times to UV irradiation.

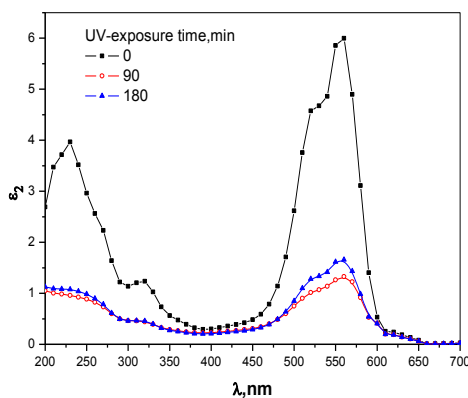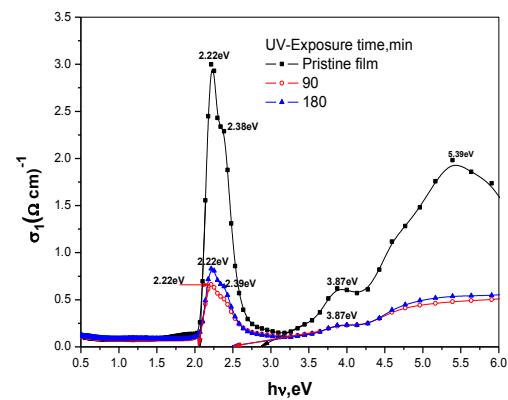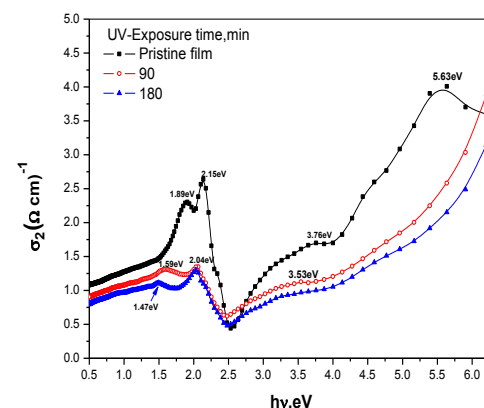**Fig 16.** Spectral distribution of σ2for RB thin films with different exposure times to UV irradiation.

Fig 14. Spectral distribution of for RB thin films with different exposure times to UV irradiation.

Fig. 16 shows the spectral distribution of σ_2 for RB thin films with different exposure times to UV irradiation. Increasing UV exposure time decreases the value of σ_2, this is attributed to

Figs. 17 and 18 show the surface energy loss, SEL, and the volume energy loss, VEL, as a

function of the incident photon energy. Both functions have the same behavior and the energy loss by photons traveling through the material is greater than the energy loss by those passing by its surface. It is clear from these figures that both of VEL and SEL follow the spectral behavior of ε_2. The UV-irradiation reduces the values of these quantities all over the spectral region under investigation. The change in their values upon irradiation can be explained in terms of the structural changes shown in Fig. 3.
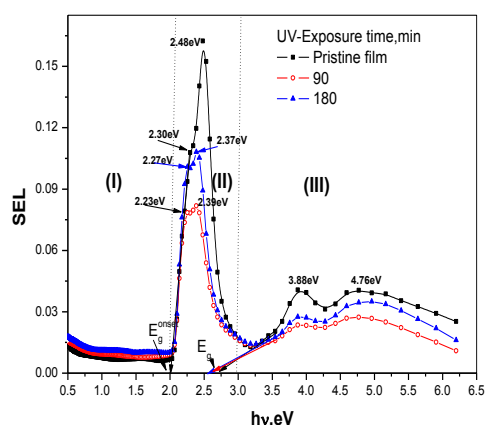

Fig 17. Spectral distribution of surface energy loss for RB thin films with different exposure times to UV irradiation.
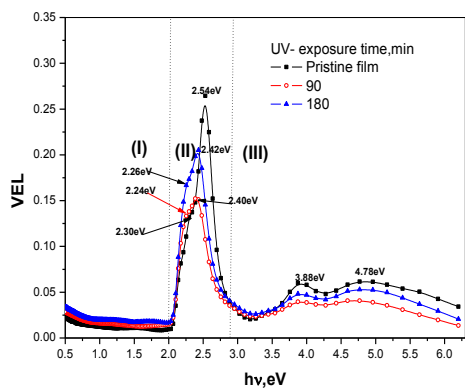

Fig 18. Spectral distribution of volume energy loss for RB thin films with different exposure times to UV irradiation.

The spectra of SEL and VEL can be divided into three regions depending on the incident photon energy: region (I) is for incident photon energy< 2eV, in this region the value of both quantities is near zero and this indicates that there is no interaction between incident photons and RB films. Region (II) is in the energy range 2-3 eV, at incident photon energy of 2eV both functions increase rapidly with photon energy

and show a shoulder and a peak around 2.3 and 2.5eV, respectively.

These peaks shift a little towards the low energy side of the VEL spectra with the increasing the irradiation time. The shoulder and peak represent vacancies, interstitials, Frenkel pairs and dislocations levels in the energy gap. Region (III) is for incident photon energy > 3eV, both of SEL and VEL show tow peaks close to 3.88 and 4.76eV represent energy levels in LUMO orbital.

Conclusions

FTIR analysis for RB films provides an evidence for its chemical stability. RB has an amorphous structure in powder and pristine film forms. Exposure of RB films to UV irradiation resulted in polymorphous polycrystalline of crystallite size that depends on UV exposure time. The data of T and R showed that homogenous optical flat films are obtained by the spin coating technique and these films can be used as optical filters. The results of calculation for n and k showed that they are independent of film thickness in the investigated thickness range of 110-500 nm and within the experimental error. High molar extinction coefficient of 5.4×10^4 (mol.cm)$^{-1}$ and broad band shown in Fig. 8 recommend RB films for application in manufacturing solar cells. The type of electron transition in RB film is indirect allowed transition and the onset and energy gaps are 2.02 and 2.85 eV, respectively. UV irradiation decreases the onset and energy gaps to 1.98 and 2.48 eV, respectively. Increasing exposure time of UV irradiation has no influence on energy gap. The dispersion parameters of RB films decrease with increasing UV exposure time.

References

Andreas B, Breunig I, Buse K, (2005) Modeling of X-ray-Induced Refractive Index Changes in Poly(methyl methacrylate). Phys. Chem. 6:1.

Baerends EJ, Ricciard G, Rosa A, Van Gisbergen SJ, (2002) A DFT/TDDFT interpretation of the ground and excited states of porphyrin and porphyrazine complexes. Coord. Chem. Rev. 230:5.

Bahadur L, Roy L, (1999) A binary mixture of dyes (2-imidazolin-5-one and Rose Bengal) for photosensitization of n-ZnO thin film electrodes in aqueous and acetonitrile media. J. Appl. Electrochem. 29:109-116.

Chang CC, Yang YT, Yang JC, Wu HD, Tsai T, (2008) Absorption and emission spectral shifts of rose Bengal associated with DMPC liposomes. Dyes and Pigments. 79:170- 175.

Cullity BD, (1978) Elements of X-ray Diffraction. Addison-Wesley Publishing company, Inc.

Davydov AS, (1971) Theory of Molecular Excitons. Plenum press, New York.

Dean JA, Ed., (1992) Langes Handbook of Chemistry, 14th Edition. McGraw- Hill, Inc., New York.

Edward PO, 1985 Hand Book of Optical Constants of Solids, Academic Press, NewYork.

El- Nahass MM, El-Gohary Z, Soliman HS, (2003) Structural and optical studies of thermally evaporated CoPc thin films. Opt. Laser Technol. 35:523-531.

El-Korashy A, El-Zahed H, Radwan M, (2003) Optical studies of [N(CH3)4]2CoCl4, [N(CH3)4]2MnCl4 single crystals in the normal para electric phase. Physica B. 334:75.

El-Mallah HM, El-Ghamaz NA and Waly MA,(2010) Influence of UV irradiation on optical properties of thermally evaporated4,4'-(1E,1'E)-2,2'-(2-aminopyrimidine-4,6-diyl)bis(ethene-2,1-diyl)bis(N,N dimethylaniline) thin films. J. Phys. D: Appl. Phys. 43:455407.

El-Menyawy EM, El-Ghamaz NA, Nawar HH,(2013) Infrared spectra, optical constants and semiconductor behavior of 5-(2-phenylhydrazono)-3,3-dimethylcyclohexanone thin films. Journal of Molecular Structure. 1036:144–150.

El-Nahaas MM, Zeyada HM, Aziz MS, El-Ghamaz NA (2002) Optical properties of thermally evaporated SnS thin films. Optical Materials.20:159-170.

El-Nahass MM, Abd El-Khalek HM, Nawar AM, (2012) Topological, morphological and optical properties of Gamma irradiated Ni (II) tetraphenyl porphyrin thin films. Optics Communications. 285:1872.

El-Nahass MM, Ammar AH, Atta AA, Farag AAM, El-Zaidia EFM, (2011) Influence of X-ray irradiation on the optical properties of CoMTPP thin films. Optics Communications. 284:2259.

El-Nahass MM, El-Deeb AF, Metwally HS, Hassanien AMH, (2011) Influence of annealing on the optical properties of 5,10,15,20-tetraphenyle-21H,23H-porphine iron(III) chloride thin films. Materials Chemistry and Physics 125:247-251.

El-Nahass MM, Youssef TE, (2010) Influence of X-ray irradiation on the optical properties of ruthenium (II)octa-(n-hexyl)- phthalocyanine thin film. J. Alloys Compd. 503:86.

El-Nahass MM, Zeyada HM, Hendi AA,(2004) Structural and optical properties of vacuum deposited thin films of (E) [α (2,5 dimethylfuryl) ethylidene] (dicyclopropyl methylene) 2,5 furadione. Optical Materials. 25:43–52

Gangotri KM, Bhimwal MK, (2010) Study the performance of photogalvanic cells for solar energy conversion and storage: Rose Bengal–d-Xylose–NaLS system. Solar Energy. 84:1294-1300

Hamza AA, Mabrouk MA, Ramadan Emara WA, AM, (2003) Refractive index and thickness determination of thin-films using Lloyd's interferometer. Optics Communications. 225:341-348

Hindeleh AM, Abdallah MA, Braik NS,(1990) Crystallinity Enhances light transmissivity through low density polyethylene sheets. J. of Materials Science. 25:1808- 1812.

Jana AK, (2000) Solar cells based on dyes. J. photochem. photobiol. A, Chem.132:1-17.

Jiang Ke-J, Xia J-b, Masaki N, Noda S, Yanagida S, (2008) Efficient sensitization of nanocrystalline TiO2 films with high molar extinction coefficient ruthenium complex. Inorg. Chim. Acta. 361:783-785.

Kim YS, Rubio V, Qi J, Xia R, Shi ZZ, Peterson L, Tung CH, O'Neill. BE, (2011) Cancer treatment using an optically inert Rose Bengal derivative combined with pulsed focused ultrasound Journal of Controlled Release. 156:315-322.

Konstantinov I, Babeva T, Ktova S, (1998) Analysis of errors in thin film optical parameters derived from spectrophotometric measurements at normal light incidence Appl. Opt. 37:4260.

Kumar GA, Thomas J, George N, Kumar BA, krishanan PR., Nampoori VP, Vallabhang CP, (2000) optical absorption studies of free (H2Pc) phthalocyanine doped borate glasses. Phys. Chem. Glasses. 41 (2):89-93.

Pradhan B, Batabyal SK, (2007) Vertically aligned ZnO nanowire arrays in Rose Bengal-based dye-sensitized solar cells. A.-J. Pal, Solar Energy Materials & Solar Cells 91:769- 773.

Pradhan B, Pal AJ,(2004) Organic heterojunction photovoltaic cells: role of functional groups in electron acceptor materials. Solar Energy Materials & Solar Cells. 81:469-476.

Roy MS, Balraja P, Kumar M, Sharma GD,(2008) Dye-Sensitized Solar Cell Based on Rose Bengal dye and nanocrystalline TiO. Solar Energy Material & Solar Cell. 92:909-913.

Roy MS, Balraju P, Kumar M, Sharma GD, (2008) Dye-sensitized solar cell based on Rose Bengal dye and nanocrystalline TiO2. Solar Energy Materials & Solar Cells. 92:909– 913

Schechtman BH, Spicer WE, (1970) Near infrared to vacuum ultraviolet absorption spectra and the optical constants of phythalocyanine and porphyrin films. J. Mol. Spectrosc. 33:28-48.

Schomaker V, Waser J, Marsh RE, Bergman G, (1959) To fit a planeor a line to a set of points by least squares. Acta Cryst. 12:600.

Sharma GD, Balraju P, Sharma SK, Roy MS, (2009)

Charge conduction process and photoelectrical properties of bulk heterojunction device based on sulphonated nickel phthalocyanine and rose Bengal, J. Physics and chemistry of solids. 70:1422-1431.

Sharma GD, Balraju P, Sharma SK, Roy MS, (2009) Charge conduction process and photoelectrical properties of bulk heterojunction device based on sulphonated nickel phthalocyanine and rose Bengal. Journal of Physics and Chemistry of Solids. 70:1422 1431

Solomon I, Schmidt MP, Sénémaud C, Khodja MD, (1988) Band structure of carbonated amorphous silicon studied by optical, photoelectron, and x-ray spectroscopy. Phys. Rev.B. 38:1326.

Szabeiski M, Luchowski R, Gryczynski Z, Kapusta P, Ortmann U, Gryczynski I, (2009) Evaluation of instrument response functions for lifetime imaging detectors using quenched Rose Bengal solutions. Chemical Physics Letters. 471:153-159.

Tauc J, (1974) Amorphous and liquid semiconductors. Plenum press, London.

Tsiper EV, Soos ZG, Gao W, Kahn A, (2002) Electronic polarization at surfaces and thin films of organic molecular crystals: PTCDA. Chem. Phys. Lett. 360:47.

Wang .J.-H, Wang .B, Liu .Q, Li. Q, Huang. H, L.Song, Sun .T.-Y, Wang H, Yu XF, Li C, Chu PK, (2013) Bimodal optical diagnostics of oral cancer based on Rose Bengal conjugated gold nanorod platform. Biomaterials. 34:4274-4283.

Weast RC, Ed ,(1975) Handbook of Chemistry and Physics, 56th Edition. CRC Press, Cleveland.

Wemple SH, DiDomenico M, (1971) Behavior of the Electronic Dielectric Constant in Covalent and Ionic Materials. Phys. Rev. B 3 (4):1338.

Yakuphanoglu F, Sekerci M, Oztuk OF, (2004) The determination of the optical constants of Cu(II) compound having 1-chloro-2,3- o- cyclohexylidine propane thin film. Opt. Commun.239:275-280.

Zeyada HM, El-Ghamaz NA, Gaml EA, (2013) Effect of substitution group variation on the optical functions of-5-sulfono-7-(4-x phenyl azo)-8-hydroxy quinoline thin films. Current Applied Physics. 13:1960-1966.

Zeyada HM, EL-Nahass MM, Elashmawi IS, Habashi AA,(2012) Annealing temperatures induced optical constant variations of methyl Violet 2B thin films manufactured by the spin coating technique. J. Non-Crystalline Solids. 358:625.

Zeyada HM, EL-Nahass MM, Samak SA,(2012) Effect of γ-ray irradiation on structure formation and optical constants of thermally evaporated rhodamine B thin films. J. Non-Crystalline Solids. 358:915-920.

Zhao G, Kozuka H, Yoko T, (1997) Effect of the incorporation of silver and gold nanoparticles Solar Energy Materials and Solar Cell on the photo anodic properties of rose bengal sensitized TiO2 film Electrodes prepared by sol-gel method. Solar Energy Materials and Solar Cell. 46:219-231.

Zhokhavets U, Goldhahn R, Gobsch G, Schliefke W, (2003) Dielectric function and one-dimensional description of the absorption of pdy(3-octylthioplene). Synthetic Metals. 138:491-495.

الملخص العربى

تأثير زمن التشعيع بالأشعة فوق البنفسجية على التركيب والخواص الضوئية للأغشية الرقيقة من زهرة بنجال

حمدى زيادة، مرتضى يوسف، ناصر الغماز، مريم ابودربالة
قسم الفيزياء – كلية العلوم – جامعة دمياط – مصر

تم بحث الخواص الضوئية للأغشية الرقيقة البكر والمشععة بالأشعة فوق البنفسجية من زهرة بنجال. تم حساب معامل الانكسار ودليل الامتصاص من القيم المطلقة لطيفى النفاذية والأنعكاسية. تم استخدام بارامترات المهتز الوحيد ونموذج درود لإمتصاص الحاملات الحرة لتحليل نتائج معامل الانكسار باستخدام نظرية الإنتقال الإلكترونى بين نطاقات الطاقة. تم تحليل الإمتصاص فى أغشية زهرة بنجال. أوضحت النتائج أن سمك الأغشية الرقيقة من زهرة بنجال لا يؤثر على معامل الإنكسار ودليل الإمتصاص وذلك فى مدى السمك الذى تم بحثه مع إدخال نسبة الخطأ فى الحسابات بعين الإعتبار.

نتج عن تشعيع الأغشية الرقيقة من زهرة بنجال بالأشعة فوق البنفسجية تغير فى التركيب حيث تحول تركيب الأغشية البكر من تركيب أمورفى إلى متعددالبلورات ونتج عن ذلك تغيير فى معامل الإمتصاص والإنكسار وفجوة الطاقة. تم حساب الدوال الضوئية واعتمادها على زمن التشعيع مباشرة من التوزيع الطيفى لثابت العزل.